University of Glasgow

Damion, R. A. et al. (2019) Quantifying T2 relaxation time changes within lesions defined by apparent diffusion coefficient in grey and white matter in acute stroke patients. *Physics in Medicine and Biology*, 64(9), 095016. (doi: 10.1088/1361-6560/ab1442)

The material cannot be used for any other purpose without further permission of the publisher and is for private use only.

There may be differences between this version and the published version. You are advised to consult the publisher's version if you wish to cite from it.

http://eprints.gla.ac.uk/182975/

Deposited on 28 March 2019

Enlighten – Research publications by members of the University of Glasgow
http://eprints.gla.ac.uk

Quantifying T_2 relaxation time changes within lesions defined by apparent diffusion coefficient in grey and white matter in acute stroke patients

Robin A. Damion[1], Michael J. Knight[1], Bryony L. McGarry[1], Rose Bosnell[2], Peter Jezzard[3], George W.J. Harston[4], Davide Carone[4], James Kennedy[4], Salwa El-Tawil[5], Jennifer Elliot[5], Keith W. Muir[5], Philip Clatworthy[2] and Risto A. Kauppinen[1]

[1]School of Psychological Science, University of Bristol, Bristol, UK; [2]Stroke Neurology, Southmead Hospital, North Bristol NHS Trust, Bristol, UK; [3]Oxford Centre for Functional MRI of the Brain, Nuffield Department of Clinical Sciences, University of Oxford, Oxford UK; [4]Acute Stroke programme, Radcliffe Department of Medicine, University of Oxford, UK; [5]Institute of Neuroscience and Psychology, Queen Elizabeth University Hospital, University of Glasgow, Scotland

Address for correspondence: Professor Risto Kauppinen
School of Psychological Science
University of Bristol
12a Priory Rd
Bristol BS8 1TU
UK
psrak@bristol.ac.uk
tel: +44 117 928 8461

Keywords: T_2 relaxation time, grey matter, white matter, diffusion MRI, acute ischaemic stroke

Running head: Onset time-dependent T_2 relaxation time change in grey and white matter

ABSTRACT

Apparent diffusion coefficient (ADC) of cerebral water, as measured by diffusion MRI, rapidly decreases in ischaemia highlighting a lesion in acute stroke patients. The MRI T_2 relaxation time changes in ischaemic brain such that T_2 in ADC lesions may be informative of the extent of tissue damage, potentially aiding in stratification for treatment. We have developed a novel user-unbiased method of determining the changes in T_2 in ADC lesions as a function of clinical symptom duration based on voxel-wise referencing to a contralateral brain volume. The spherical reference method calculates the most probable pre-ischaemic T_2 on a voxel-wise basis, making use of features of the contralateral hemisphere presumed to be largely unaffected. We studied whether T_2 changes in the two main cerebral tissue types, i.e. in grey matter (GM) and white matter (WM), would differ in stroke.

Thirty-eight acute stroke patients were accrued within 9 hours of symptom onset and scanned at 3T for 3D T1-weighted, multi b-value diffusion and multi-echo spin echo MRI for tissue type segmentation, quantitative ADC and absolute T_2 images, respectively. T_2 changes measured by the spherical reference method were 1.94 ± 0.61, 1.50 ± 0.52 and 1.40 ± 0.54 ms/hour in the whole, GM and WM lesions, respectively. Thus, T_2 time courses were comparable between GM and WM independent of brain tissue type involved. We demonstrate that T_2 changes in ADC-delineated lesions can be quantified in the clinical setting in a user unbiased manner and that T_2 change correlated with symptom onset time, opening the possibility of using the approach as a tool to assess severity of tissue damage in the clinical setting.

1. INTRODUCTION

Ischaemia resulting in catastrophic energy failure followed by anoxic depolarization, causes a dramatic drop in the apparent diffusion coefficient (ADC) of water, which enables detection of ischaemic stroke in the brain by diffusion MRI (Moseley *et al.*, 1990; Busza *et al.*, 1992). In acute strokes, brain parenchyma with an ADC lowered by more than 20% is commonly considered as the ischaemic core (Hossmann, 1994; Burgess and Kidwell, 2011). MRI relaxation time changes in the ischaemic core are very small in magnitude in the early moments of ischaemia (Kauppinen, 2014). However, recent evidence points to a potential value of relaxation times in stroke onset time evaluation (Siemonsen *et al.*, 2009; Jokivarsi *et al.*, 2010; McGarry *et al.*, 2016). Combined diffusion and relaxometric MRI would therefore bear an impact on stroke patient stratification, keeping in mind that up to 30% of acute patients present with unknown onset (Thomalla *et al.*, 2011). While diffusion MRI contrast is conspicuous to the naked eye in acute stroke, T_2-weighted or quantitative T_2 MRI signals become brighter only many hours after symptom onset which is often outside the time window for treatment with thrombolysis. The so-called diffusion/FLAIR MRI mismatch, which exploits qualitative signal intensities of diffusion and T_2-weighted images, has been successfully used to stratify stroke patients within the thrombolysis time window of 4.5 hours (Thomalla *et al.*, 2011; Thomalla *et al.*, 2018). Similarly to T_2-weighted signal, the quantitative T_2 relaxation time image also shows weak contrast in early hours of stroke, thus requiring special means to measure the effects of ischaemia on quantitative T_2. The mirror reference approach uses an anatomically homologous contralateral brain volume as a non-ischaemic reference to measure a difference in quantitative T_2 in the ADC-defined ischaemic core (Siemonsen *et al.*, 2009). Using the mirror reference procedure, it has been shown that quantitative T_2 at 1.5T increases by ~10% by 4 hours after symptom onset in brain parenchyma, providing a means to estimate lesion age within the thrombolysis time window (Siemonsen *et al.*, 2009). The mirror reference approach requires precise positioning of non-ischaemic reference into intact brain parenchyma (Norton *et al.*, 2017), which is not often straightforward in aged human brain.

The brain parenchyma consists of two main tissue types, grey matter (GM) and white matter (WM), having greatly different cell and biochemical compositions, receptor distributions, electrophysiology, metabolic rates of oxygen and glucose, and haemodynamics. Because of these fundamental neurobiological differences, these two brain tissue types show inherently different T_1 and T_2 relaxation time values resulting in contrast in respective MR images. ADC

values are quantitively comparable in GM and WM and, consequently, orientation-unbiased ADC images show little contrast between these tissue types. Whether the above-mentioned quantitative MRI parameters have different time courses in GM and WM following stroke remains to be studied. Diffusion MRI of rat brain shows a dramatic drop in ADC when cerebral blood flow (CBF) reduces by approximately 80% (Hossmann, 1994; Grohn *et al.*, 2000). Recent studies on human stroke patients using either perfusion MRI (Bristow *et al.*, 2005) or perfusion computerized tomography (CT) (Chen *et al.*, 2017) in combination with diffusion MRI reported that CBF thresholds for the ischaemic core in GM is higher than in WM. In addition to different haemodynamic thresholds to ischaemia, anoxic depolarizations show different kinetics in the two tissue types. Anoxic depolarisation in ischaemic feline GM attains the lowest values in 5 – 10 minutes, whereas in WM it reaches the minimum by ~30 – 40 minutes (Kumura *et al.*, 1999). Anoxic depolarization is associated with a shift of water from the extracellular into the intracellular space, i.e. cytotoxic oedema, which is one of key factors leading to a decrease both in ADC (Sotak, 2002) and T_2 relaxation rate (Knight *et al.*, 2015). In global ischaemia in cats, ADC in the thalamus (representing GM) decreases with a time constant that is three-fold faster than in the internal capsule (representing WM) (Pierpaoli *et al.*, 1996) in accordance with the anoxic depolarization data (Kumura *et al.*, 1999). In the light of these observations it would be of clinical interest to determine stroke onset time-dependent quantitative T_2 changes in GM and WM to deduce the best use of this MRI indicator for brain tissue state assessment in stroke patient management.

In the present paper we present a novel method to measure T_2 relaxation time change as a function of stroke onset time in mixed tissue type lesions, as well as in GM and WM separately, in the ADC-defined ischaemic core. The approach is called the spherical reference method which, with the aid of T_2-weighted MR images, is based on a voxel-level search for contralateral, non-ischaemic, reference sphere voxels that are optimally matched to the parenchyma that is affected by stroke. We have used both the spherical and mirror reference approaches (Siemonsen *et al.*, 2009) to quantify effects of acute stroke on quantitative T_2 in the ADC-defined stroke lesion.

2. Methods

2.1. Human data acquisition and processing

The study received ethical approval to accrue acute stroke patients from South West Frenchay Research Ethics Committee for participants in Bristol (ref 13/SW/0256), Scotland A REC for participants in Glasgow (ref 16/SS/0223) and UK National Research Ethics Service committees (ref: 12/SC/0292 and 13/SC/0362) for participants in Oxford. Informed consent was received either from participants or their legal representative prior to enrolment to the study. Stroke patients were recruited if they presented in the emergency department with witnessed symptom onset so that MRI scans could be completed within 9 hours of onset. Details of the human acute stroke cohort is given in Table 1. The project was carried out in accordance with the Declaration of Helsinki.

All MRI scans on acute stroke patients were acquired using 3T scanners: Philips Achieva (Bristol); Siemens Magnetom Prisma (Glasgow); Siemens Magnetom Verio (Oxford). At each of the three sites, a 32-channel head-coil was used. The details of the T_1, diffusion, and T_2 pulse sequences and acquisition parameters are given in Table 2.

Quantitative T_2 maps were obtained by fitting a mono-exponential decay on a voxel-wise basis. All T_2-weighted images of the echo-series were summed to produce a sum-over-echoes image, which was subject to bias-field correction (Zhang *et al.*, 2001) using FSL FAST (FMRIB, Oxford, UK).

For diffusion MRI data using three orthogonal diffusion-sensitising gradients at a common b-value, orientation-independent apparent diffusion coefficient (ADC) maps were obtained from

$$ADC = -\ln(S_1 S_2 S_3 / S_0^3)/3b$$

where $S_{1,2,3}$ are the signal intensities at the three orthogonal directions, S and S_0 are the signal intensities with (b = 1000 s/mm^2) and without (b = 0) diffusion weighting respectively and b is the b-value.

Diffusion-weighted data with twenty independent diffusion-gradient directions (b=1000 mm^2/s) and three b=0 images were processed using FSL DTIFIT from which the resulting mean-diffusivity maps provided the ADC values.

2.2. Image registration

Firstly, brain-extracted ADC images were non-linearly registered to the T_2-weighted image space using FSL FNIRT via the diffusion S_0 image and the T_2 sum-over-echoes image. If T_1-weighted images were available, the T_2-weighted image space was then linearly (six degrees of freedom) registered to the T_1-weighted image space and then the latter space was linearly registered to the MNI frame at 1 mm^3 isotropic resolution, using FSL FLIRT (Jenkinson and Smith, 2001). If T_1-weighted images were not available, instead, the T_2-weighted image space was linearly registered directly to the MNI frame at 1 mm^3 isotropic resolution. All relevant images were then linearly registered to the MNI frame using the registration maps (or combinations of maps) generated by the previous stages.

2.3. Lesion identification and mask creation

A reference tissue mask was first created by the application of thresholds on T_2 and *ADC* to reduce the contribution from CSF. These thresholds were typically 30 ms < T_2 < 200 ms and 0.1 $\mu m^2\ ms^{-1}$ < *ADC* < 1.5 $\mu m^2\ ms^{-1}$, respectively. A lesion tissue mask was then created in two stages. First, the thresholds (which could vary in individual cases) 30 ms < T_2 < 200 ms, 0.2 – 0.4 $\mu m^2\ ms^{-1}$ < *ADC* < 0.55 – 0.60 $\mu m^2\ ms^{-1}$ were applied and, secondly, the additional criterion that the *ADC* should be less than one half-width half-maximum from the median *ADC* of the reference tissue was applied. The lesion mask was then further refined by removing all but the largest contiguous cluster (or clusters, in cases with more than one lesion). Subsequently, the lesion mask was then removed from the reference tissue mask to create a non-lesion tissue mask.

In order to examine GM and WM tissue only, further masks were created. GM and WM masks were obtained using FSL FAST with the T_2-weighted, sum-over-echoes image as input, and specifying four tissue-types to be segmented. If available, T_1-weighted images were used to generate a subcortical-structures mask via FSL FIRST. This mask was subtracted from the GM and WM masks to produce purely cortical GM and WM masks. These resulting masks were logically combined with the lesion and non-lesion tissue masks when investigating the tissue types separately. All masks were inspected visually. Note that when total lesions (‘all tissue’) were investigated, these masks were not employed.

2.4 Algorithm for T_2 change due to ischaemia: Spherical Reference method

To calculate the change in T_2 due to ischaemia for each voxel in the lesion, it is necessary to provide reference, T_2^R, values to which each voxel’s ischaemic T_2 can be compared. That is,

an estimate is needed for the *pre*-ischaemic T_2 within each voxel of the lesion. Reference T_2 values have previously been obtained (Siemonsen *et al.*, 2009; Jokivarsi *et al.*, 2010) from single contralateral voxels in the unaffected hemisphere, the so-called mirror reference method. However, such a method is prone to error due to the imperfect symmetry and inherent heterogeneity of the human brain, particularly in older patients and patients with cerebrovascular disease where T_2 hyperintense WM lesions are common. To circumvent this issue, pre-ischaemic (reference) T_2^{R} values are calculated (via T_2-weighted MR images) from a spherical volume of a given radius, centred on the contralateral voxel in the unaffected hemisphere.

To achieve this, the algorithm adopts the premise that, in the hyperacute phase of ischaemia, the T_2-*weighted* images are relatively insensitive to ischaemia and therefore the intensity values within each voxel of the lesion are sufficiently close to their pre-ischaemic values to be taken as estimates for their pre-ischaemic values (Welch *et al.*, 1995; Moseley *et al.*, 1990; McGarry *et al.*, 2016). With this premise, the intensity I^{L} of a lesion voxel can be used to condition the reference T_2 for that voxel.

Despite the relative insensitivity to ischaemia of the T_2-weighted intensities, there may still be a dependency between the intensities and T_2 values in normal brain tissue within any given region. Therefore, it is possible to obtain an estimate of pre-ischaemic T_2 by using the intensity estimate of the pre-ischaemic intensity (i.e., the ischaemic intensity value I^{L}) to calculate a type of conditional expectation of the T_2 values within the reference sphere of a given lesion voxel. That is, an estimate of the pre-ischaemic T_2 is obtained from the mean T_2 of normal brain tissue within a reference sphere, conditioned by the intensity value I^{L} of the ischaemic lesion voxel.

To effect the conditioning, we employ a penalty function $F_{\mathrm{L}}(I)$ which weights the sum over the T_2 values associated with voxels, indexed by ρ, in the reference sphere S_{L}. Therefore, let the T_2^{R} be given by

$$T_2^{\mathrm{R}} = \sum_{\rho=1}^{N_{\mathrm{S}_{\mathrm{L}}}} T_{2,\rho} F_{\mathrm{L}}(I_\rho)$$

where $N_{\mathrm{S}_{\mathrm{L}}}$ is the number of voxels in the reference sphere S_{L}, and where the penalty function is normalised by $\sum_{\rho=1}^{N_{\mathrm{S}_{\mathrm{L}}}} F_{\mathrm{L}}(I_\rho) = 1$. This may be equivalently expressed as

$$T_2^{\mathrm{R}} = \frac{\langle T_2 F_{\mathrm{L}}(I)\rangle}{\langle F_{\mathrm{L}}(I)\rangle} = \frac{\int \mathrm{d}I\, F_{\mathrm{L}}(I)P(I) \int \mathrm{d}T_2\, T_2 P(T_2|I)}{\int \mathrm{d}I\, F_{\mathrm{L}}(I)P(I)} = \frac{\int \mathrm{d}I\, F_{\mathrm{L}}(I)P(I)\langle T_2|I\rangle}{\int \mathrm{d}I\, F_{\mathrm{L}}(I)P(I)}$$

where the integrals are over the values contained in the reference sphere, $P(I)$ is the probability density for the intensities, $P(T_2|I)$ is the conditional probability density for T_2 given the intensity I, and $\langle T_2|I\rangle$ is the mean T_2 conditioned on I.

In the limit that $F_{\mathrm{L}}(I)$ is constant, T_2^{R} is the unweighted mean T_2 of all the voxels in the reference sphere. Conversely, in the limit that $F_{\mathrm{L}}(I)$ becomes a delta-function positioned at $I = I^{\mathrm{L}}$, then $T_2^{\mathrm{R}} = \langle T_2|I^{\mathrm{L}}\rangle$. However, in the present context, the use of a delta-function is impractical. Instead, a penalty function of finite width is employed, such that

$$F_{\mathrm{L}}(I_\rho) = A_{\mathrm{L}}\exp\left(-\left[\frac{I_\rho - I^{\mathrm{L}}}{I^{\mathrm{L}}}\right]^2/2\sigma^2\right)$$

where A_{L} is a normalisation constant which depends on the reference sphere S_{L} associated with each lesion voxel. With this penalty function, T_2^{R} can be regarded as the mean T_2 within the reference sphere, conditioned on a Gaussian neighbourhood of I^{L}.

Thus, for a given lesion voxel with intensity I^{L} and T_2-value T_2^{L}, from its reference sphere (centred on the contralateral voxel) we can obtain a reference T_2-value T_2^{R}. We can therefore compute a measure of the estimated change in T_2 due to ischaemia as a difference $\Delta T_2 = T_2^{\mathrm{L}} - T_2^{\mathrm{R}}$ or a ratio $rT_2 = T_2^{\mathrm{L}}/T_2^{\mathrm{R}}$ for each lesion voxel, and use the median of these changes as an overall measure of the change in the ischaemic lesion. This method can also be used to estimate changes in other MRI parameters, such as the ADC value, provided that the distributions of this parameter and the intensity values are not statistically independent.

In our implementation of this algorithm, the T_2-weighted intensities were obtained from the sum-over-echoes image after bias-field correction. The reference sphere radius and penalty function width, σ, were obtained by optimisation on each patient data set by using the unaffected tissue in the hemisphere of the lesion (via the non-lesion tissue mask) to minimise the function $f(\beta) = \mathrm{MAD}(\Delta T_2) + \beta|\mathrm{med}(\Delta T_2)|$, with $\beta = 5$, where ΔT_2 is the calculated change in T_2, $\mathrm{med}(\Delta T_2)$ is the median, and $\mathrm{MAD}(\Delta T_2)$ is the median absolute deviation. Median values for the reference sphere radii and penalty function width are provided in the Supplementary Material, Tables S1 and S2.

A work-flow for image post-processing, the creation of various masks and use of these masks and images as inputs to the spherical reference algorithm, is shown in Figure 1.

2.5 Mirror Reference method

We used the method essentially as proposed by Siemonsen et al. (Siemonsen *et al.*, 2009) to determine a reference volume from the contralateral, non-ischaemic hemisphere, but without the need for manual adjustments. Since all image processing was performed in the MNI frame, the midline of the brain was consistently defined. Therefore, the lesion mask (see section above) could simply be reflected about the midline and then logically combined with the non-lesion tissue mask to ensure that this contralateral (mirror reference) mask also contains valid tissue. To investigate GM and WM separately, the same operations were performed on these masks after logically combining with the GM and WM segmentation masks (see section 2.3). T_2 statistics could then be easily compared between the lesion and the contralateral mask regions.

2.6 Weighted regression analysis and statistics

Weighted, least-squares, linear regressions were used to analyse the results obtained from the spherical and mirror reference methods, and the lesion ADC (median) values. The weights used for the regressions were the inverse-square errors of the medians (or combinations or medians). The errors for the medians were determined using the method of McKean and Schrader (McKean and Schrader, 1984; Price and Bonett, 2001) which derives the errors from the 95% confidence intervals of the distributions.

The order of calculations for quantities of interest is slightly different when comparing the spherical and mirror reference methods. In the former method, differences or ratios are formed for each lesion voxel, producing a distribution from which measures can be obtained, namely, median values, MADs, and errors in the medians. We note here that the errors in the medians tend to be close to $1.48\sqrt{\pi/2N}$ MAD, where N is the number of voxels in the lesion, which is the relationship expected when the distribution is Gaussian. In contrast, in the mirror reference method, quantities of interest are first calculated from the two regions; the lesion and contralateral reference. The medians are then combined as a difference or ratio. MADs and errors in medians, however, are propagated (in the usual manner for independent measures of error) for the difference or ratio of medians from the two regions. If the same order of calculations was followed for the spherical reference method, a second set of optimised penalty function parameters would have been required for this alternative procedure.

Using a bootstrap method, it was found that of the order of at least 20 voxels were required to determine reasonably accurate estimates for the errors. Therefore, prior to performing the weighted regression, data were rejected if their region voxel count (whether connected or not)

was less than 20 (which corresponds to a volume of 20 mm^3). For the mirror reference method, this test was applied to both the lesion and contralateral reference region.

All weighted regressions were performed within MATLAB (Release 2016b, The MathWorks, Inc., Natick, MA, United States) using *fitlm*, which returns all regression parameters, confidence intervals, and significance tests. In order to compare regressions between GM and WM, the two data sets were concatenated and weighted regressions were performed with four parameters $\{a, b, c, d\}$ such that the dependent variable y was fitted to $y = a + bT + \gamma(c + dT)$, where T is the onset time, and $\gamma = 1$ for the GM data, and $\gamma = 0$ for the WM data. The fitted parameters c and d are the differences between the GM and WM intercepts and gradients, respectively, and thus can be subjected to a significance test for the null hypothesis, which *fitlm* provides.

3. RESULTS

ADC and quantitative T_2 images from four stroke patients with lesions involving different vascular territories are shown in Figure 2. Stroke lesions present as hypointense volumes in ADC images compared to the surrounding tissue. The stroke lesions' boundaries are shown on the ADC images [Figure 2(a), (c), (e), and (g)] from which they were derived. Superimposed on the T_2 images [Figure 2(b), (d), (f), and (h)] are the lesions segmented into GM and WM tissue types.

Low ADC is a well-established MRI biomarker for ischaemia in the human brain (Welch *et al.*, 1995; Hjort *et al.*, 2005; Burgess and Kidwell, 2011). The median ADC in the total lesions [Figure 3(a)], segmented GM [Figure 3(b)], and WM [Figure 3(c)] are shown as a function of onset time (see Table 3 for regression data). The ADC values are within the range reported for an ischaemic core in all volumes at the time of MR scans in the hyperacute phase of stroke, and the low ADC was the primary MRI criterion for assigning the lesion to ischaemic core (both in thrombolysed and not thrombolysed patients, Table S3). However, a low diffusivity lesion may be transient, and therefore it may not be a genuine core (Kranz and Eastwood, 2009). To address this issue, a subcohort of patients consented for a follow-up MRI 1 – 4 days after symptom onset. ADC lesion volumes for both hyperacute and follow-up MRI are shown in Figure 4. It is evident that on average the ADC lesions expanded from 1st to 2nd scan (Table 1). However, a tendency towards volume decline was measured in 5 cases (31% of patients with follow-up scans), 4 of which were thrombolysed. Based on these data from the follow-up MRI, the ADC lesion in the hyperacute phase was regarded to represent the ischaemic core in 69% of all patients.

Three quantities for quantitative T_2 were examined for the total lesion (*All Tissue* in Figure 5), GM, and WM using the spherical reference method: $\mathrm{med}(\Delta T_2)$ [Figure 5(a) – (c)]; $\mathrm{med}(rT_2)$ [Figure 5(d) – (f)]; and $\mathrm{med}(rI)$ [Figure 5(g) – (i)]. It can be seen that both $\mathrm{med}(\Delta T_2)$ and $\mathrm{med}(rT_2)$ showed an increasing trend as a function of onset time, whereas the slope of $\mathrm{med}(rI)$ was not significantly different to zero. Table 4 summarizes the quantified parameters for the three MRI measures in the total lesion, GM, and WM.

For the two measures of quantitative T_2 change, GM and WM values correlated well with onset time, with gradients 1.4 – 2.0 ms h^{-1} for $\mathrm{med}(\Delta T_2)$, and 0.011 – 0.020 h^{-1} for $\mathrm{med}(rT_2)$. Trends and statistics were similar for both of these measures. T_2 changes as a function of stroke onset

time (median ± 95% confidence bounds) measured by the spherical reference method were 1.94 ± 0.61, 1.50 ± 0.52 (p = 0.38 vs. the whole lesion) and 1.40 ± 0.54 (p = 0.18 vs the whole lesion) ms/hour in the whole, GM and WM lesions, respectively. For $\mathrm{med}(rI)$, the gradient was not statistically different to zero. For all quantities investigated with the spherical reference method, no significant differences in intercept or gradient were found between WM and GM.

Figure 6 shows the T_2 data obtained by the mirror reference method as follows: Figure 6(a) – (c), $\mathrm{med}(T_2^{\mathrm{L}}) - \mathrm{med}(T_2^{\mathrm{R}})$, (the difference in median T_2); Figure 6(d) – (f), $\mathrm{med}(T_2^{\mathrm{L}})/\mathrm{med}(T_2^{\mathrm{R}})$, (the ratio of median T_2), and Figure 6(g) – (i), $\mathrm{med}(I^{\mathrm{L}})/\mathrm{med}(I^{\mathrm{R}})$, (the ratio of median T_2-weighted intensities). Positive slopes were evident for all volumes studied both for $\mathrm{med}(T_2^{\mathrm{L}}) - \mathrm{med}(T_2^{\mathrm{R}})$ and $\mathrm{med}(T_2^{\mathrm{L}})/\mathrm{med}(T_2^{\mathrm{R}})$. A tendency to a positive slope can be seen also for $\mathrm{med}(I^{\mathrm{L}})/\mathrm{med}(I^{\mathrm{R}})$. Quantitative indices for fitted regression lines are given in Table 4.

For the two measures of quantitative T_2 change that were used in the mirror reference method, GM and WM data correlated well with onset time, with gradients 1.6 – 3.2 ms h^{-1} for the difference of medians, and 0.016 – 0.028 h^{-1} for the ratio of medians. Trends and statistics were similar for both of these measures. For the intensity ratio, the gradient was statistically significant with values 0.008 – 0.013 h^{-1}. For all quantities investigated with the mirror reference method, no significant differences in intercept or gradient were found between WM and GM.

For analogous measures of quantitative T_2 change between the spherical and mirror reference methods, the general trends were similar but the 95% confidence intervals, p-values, and RMSE tended to be smaller for the spherical reference method. For the intensity ratios, however, while the mirror reference method produced significant trends, the spherical reference method did not. The 95% confidence intervals and RMSE were also much smaller in the latter method.

The patients recruited to the study were treated according to the NHS standard-of-care protocols, thus recombinant plasminogen activator was administered to eligible patients often prior to MRI. Linear regression characteristics for quantitative T_2 data are also presented separately for thrombolysed and not thrombolysed patients (Table S4). It is evident that while ΔT_2 as determined by both methods showed highly significant correlation with onset time in thrombolysed patients, it was not different from zero in not thrombolysed cases (Table S4). Thrombolysis is not given to patients with mild and small strokes and we believe that non-significant T_2 change within the time frame up to 9 hours reflected mild disease states.

4. DISCUSSION

We have developed a robust and user-unbiased procedure to quantify effects of stroke on T_2 relaxation time in the ADC-defined ischaemic core and have applied it to MRI data from a cohort of acute ischaemic stroke patients. The quantitative T_2 changes measured by the spherical reference method, as a function of symptom onset time, agree well with those determined by the recently-introduced mirror reference method, which was the first method to objectively measure the effect of ischaemia on T_2 relaxation time both in preclinical (Jokivarsi *et al.*, 2010; McGarry *et al.*, 2016) and clinical (Siemonsen *et al.*, 2009) data sets. Our results show that increase in T_2 relaxation time in quantitative terms is similar both in GM and WM to ischaemia with symptom onset time, an observation that may have potential value in interpreting MRI scans of stroke patients.

While the reduction of ADC due to ischaemia has a large dynamic range, making it conspicuous by the bare eye, effects of ischaemia on T_2 are small, requiring special referencing to non-ischaemic brain parenchyma to become detectable. The mirror reference method, wherein a homologous contralateral brain volume is chosen, utilises anatomical criteria for selection of a non-ischaemic reference region to determine the difference of average T_2s. Using the mirror reference in rodent models, it was reported that T_2 initially shortens both in the ischaemic core and parenchyma surrounding the core, the so-called ischaemia expansion tissue, followed by a time-dependent prolongation (Jokivarsi *et al.*, 2010). The temporal behaviour of T_2 during the first hours has been attributed to cytotoxic edema (linked to anoxic depolarisation) followed by disintegration of intracellular macromolecules by proteases and lipases; the so-called cytotoxic edema dissociation model (Knight *et al.*, 2015). The ΔT_2 data as a function of symptom onset obtained by both the spherical and mirror reference methods here indicate that ΔT_2 may be negative also in human brain in the early hours of stroke. Interestingly, Siemonsen and coworkers (Siemonsen *et al.*, 2009) reported only positive ΔT_2 by the mirror reference approach in acute stroke patients scanned at 1.5T. Reasons for the discrepancy of ΔT_2 data between the two studies remains unknown to us,, however, that the mirror reference method is critically dependent on accurate delineation of the reference volume (Norton *et al.*, 2017), which may not be always obtainable in the human brain, as well as on the absence of any pathology in the reference that may affect T_2. The latter factor becomes a serious concern in stroke patients, who often are aged with neurological co-morbidities that may influence MRI parameters.

The spherical reference method was designed to minimise the effects of potential confounds caused by brain asymmetry and tissue pathology in the reference volume, and also to make the reference selection user-unbiased. Reference volume delineation is based on T_2-weighted signal intensity in the voxels of the ADC-defined lesion by seeking matching voxels in the contralateral hemisphere. Experimentally, T_2-weighted signal shows no time-dependency in the ischaemic core of rat stroke for approximately the first 5 hours (Knight *et al.*, 2015). In stroke patients, T_2-weighted hyperintensity is commonly present only hours or days after symptom onset. Therefore, it is reasonable to use the T_2-weighted signal in the ADC lesion during the first hours of stroke as a starting point in the search of a non-ischaemic reference.

In the spherical reference method, there are two parameters associated with the penalty function that are optimised for each patient data set: the radius of the reference sphere and the penalty function width (Tables S1 and S2 for optimised parameter values). The optimisation procedure assumes that if the spherical reference method is used to calculate $\mathrm{med}(\Delta T_2)$ between two hemispheres of normal brain tissue the result should be approximately zero. However, there are at least two reasons why this assumption is not straightforward, and one or more of these could be the cause of the large range of optimised parameter values (Table S1). Firstly, normal tissue needs to be properly identified. In the current method, this is achieved by creating a non-lesion mask by removing the lesion mask from the brain mask (with CSF areas removed by applying an upper T_2 limit). This simple method has obvious weaknesses: for example, in assuming that all the ischaemic lesions have been identified, or in assuming that the region affected by ischaemia is entirely within the ADC-defined region, or by assuming that there are no other pathologies present. In patients with white matter T_2 hyperintensities there is some suggestion that their presence in images might affect the optimised parameters (Table S2). Secondly, presumably due to imperfect bias-field correction (but perhaps also other issues or tissue characteristics), a zero-crossing for $\mathrm{med}(\Delta T_2)$ (as a function of reference sphere radius and penalty function width) is not always observed. For this reason, and also in the case where more than one zero-crossing is observed, the function $\mathrm{MAD}(\Delta T_2) + 5|\mathrm{med}(\Delta T_2)|$ is minimised instead. A further point of concern with the current implementation of the optimisation is its lengthy execution time which, in addition to the other stages of the spherical reference method, would render the method of limited value in a clinical setting. Nonetheless, there is hitherto unexplored scope for improved efficiency, for example in reducing the number of normal-brain voxels required, or in employing smarter optimal-parameter search algorithms.

ΔT_2 data as a function of symptom onset do not obviously differ when analysed by the two methods (Table 4). However, the spherical reference method shows smaller variation (95% confidence intervals on fitting parameters and regression lines) and RMSEs that are, throughout, substantially lower than by the mirror reference approach, indicating that the former is more robust in selecting non-ischaemic tissue that is similar to that affected by stroke. Median absolute deviations (displayed as 'error' bars in Figures 5 and 6) also tend to be smaller in the spherical reference method, as do the errors in the median values (used for the weighted regressions), which also imply that the voxel-selectivity at the centre of this method improves precision while maintaining accuracy.

The order of (final) calculations for quantities of interest is different between the mirror and spherical reference methods. In the mirror reference method, median values are obtained from the lesion and mirror regions before combining these two values into a ratio or difference. The spherical reference method, however, is designed to place more importance on calculations at a voxel-wise level. In doing so, images of T_2 change (such as the ΔT_2 image in Figure 1) or histograms of T_2 change in lesions or surrounding tissue (not shown) can be produced and analysed in terms of magnitude and spatial extent with regard to the ADC-defined lesion (or other images). This requires calculating the ratio or difference for each voxel in the lesion (or entire ipsilateral hemisphere) before any summarising median value is obtained. Thus, the order of final calculations is different for the proposed spherical reference method (ratio or difference, then median) to the mirror reference method (median values, then ratio or difference). It should be noted, nonetheless, that both methods can, in principle, be modified so that the final calculations have the same order. The mirror reference method can be changed so that each lesion voxel is combined with its contralateral voxel (assuming it exists) before taking the median of the combined values. The spherical reference method can be altered such that medians can be calculated from the lesion region and from the calculated reference T_2^{R} values before combining them. The disadvantage of the modified mirror reference method is that it becomes more sensitive to mismatches in tissue types between ipsilateral and contralateral voxels. The disadvantage of the modified spherical reference method is that the ability to produce images or histograms of T_2 change is lost (note that it is likely that the optimised penalty function parameters will be different in the modified method).

Comparing the measures of T_2 change (Table 4) between GM and WM in the mirror reference method, it is observed that there is more variability in the figures for GM than for WM.

Unambiguously establishing which voxels are those primarily containing GM tissue can be problematic, particularly when analysing images which have undergone one or more spatial (registration) transformations. This, in addition to the known variability associated with the exact placement of the contralateral reference region, could be the main reasons for the larger uncertainty in the GM results. In this regard, it is interesting that the results of the spherical reference method do not appear to exhibit this tendency. This could be attributable to the reduced reliance of this method on the contralateral voxel positions and its voxel-matching feature. Nonetheless, both methods could potentially be improved by incorporating the partial-volume information obtained from the segmentation procedure (FSL FAST).

Our data show that time courses of ΔT_2 in GM and WM are similar as a function of stroke symptom onset. At first glance, this is unexpected in the light of animal studies which have demonstrated different time dependencies in anoxic depolarisations (Kumura *et al.*, 1999) and ADC (Pierpaoli *et al.*, 1996) in the two brain tissue types. It should be realised, however, that there are several fundamental experimental differences between our clinical data and those from animal studies. Firstly, in the current study the earliest time points for MRI were obtained around 140 minutes after symptom onset, thus, no very early MRI data of stroke were available to us. Secondly, CBF thresholds for neurological symptoms and ischaemic energy failure (which triggers the drop in ADC) are different (Hossmann, 1994). Preclinical studies have shown that spontaneous electrical activity becomes disrupted at CBF levels that are 50 – 60% below the physiological level (Hossmann, 1994), whereas the ADC drop has a flow threshold that is approximately 80% below the normal flow (Busza *et al.*, 1992). These CBF thresholds are time-dependent so that the ADC may decrease at a higher CBF level over a period of time than if the occlusion is instantaneous. Thus, the preclinical studies have reported electrophysiological and ADC data as a function of ischaemia, whereas in our clinical cohort the exact onset of ischaemia remains unknown, notwithstanding the ostensible symptom onset time.

Limitations

Prior to drawing conclusions regarding potential clinical implications of the current methodology and data in stroke medicine, several limitations should be considered. Firstly, the sample size is modest, comprising of a heterogeneous distribution of involved vascular territories. It is impossible to conclude, from the current data set, whether ΔT_2 as a function of onset time is quantitatively uniform in different vascular territories. Secondly, the majority of patients in the current cohort (66%) were thrombolysed prior to MRI. Recanalization may or

may not normalise ADC (Li *et al.*, 1999) or T_2 (Kettunen *et al.*, 2002) depending on the duration of ischaemia. Preclinical data demonstrate that if recanalization is successful, ADC recovers and T_2 overshoots transiently (Kettunen *et al.*, 2002), but if ADC remains low, T_2 increases with time producing a prolonged T_2 (Li *et al.*, 1999). We have used the same ADC criterion for all patients to delineate the lesion, and furthermore, as the follow-up MRI data from thrombolysed patients indicate that the size of the ADC lesions increased in 11 out of 16 cases, we assumed that thrombolysis prior to first MRI had minimal or no effect on lesion T_2. Thirdly, the three hospitals that were involved in this study used two types of MRI pulse sequences to quantify T_2 in humans, which yield different absolute T_2 values from brain parenchyma (this was partly the reason for considering ratio measures as well as difference measures of T_2 change). The critical parameter used in determining the effects of stroke is ΔT_2. However, in the current data set it is impossible to separate ΔT_2s in ADC lesions measured by either of the two MRI methods.

In spite of the limitations above, the current data have potential clinical implications warranting further investigation. Firstly, quantitative ADC and T_2 in combination may offer an objective way to evaluate effects of stroke on brain tissue, aiding in patient stratification. Recent clinical studies have used DWI/T_2-FLAIR signals to evaluate lesion age (Thomalla *et al.*, 2009; Thomalla *et al.*, 2018). The approach exploits a higher signal intensity arising due to the lengthened T_2 and increased proton density as a proxy of lesion age. However, this signal increase may be counteracted by a T_1 contribution, which increases with time after onset in the first hours in animal models (Kauppinen, 2014; McGarry *et al.*, 2016), decreasing the FLAIR signal. "DWI/T_2-FLAIR" mismatch as a proxy of lesion age is commonly determined visually, being classified by a binary value of whether or not a FLAIR and DWI lesion can both be seen (Thomalla *et al.*, 2011). In a trial of 643 patients, it was shown that in the time range 181 – 270 minutes, 53% of patients present a mismatch and 47% do not, and that patients with no mismatch, who would otherwise be ineligible for thrombolysis, greatly benefited from treatment (Thomalla *et al.*, 2018). The spherical reference approach may provide even more quantitative information on the age of stroke lesions than visually-determined DWI/T_2-FLAIR mismatch in an unambiguous manner, but the latter approach is pending a clinical trial. Secondly, stroke onset time-dependent T_2 changes in GM and WM are comparable within the time window studied here. Therefore, T_2 relaxation time serves as a proxy of tissue state independently of the brain tissue type in the ADC lesion volume. It should be noted that the situation may be different when T_2-weighted intensities are used, due to potential contribution by T_1 in scan acquisitions and the inherently distinct T_1s in GM and WM.

5. CONCLUSIONS

We have introduced a novel user-independent spherical reference method to quantify T_2 relaxation time changes in acute ischaemic stroke lesions with low ADC, both in GM and WM volumes. Using this technique, ΔT_2 increases by 1.4 – 1.5 ms/h in both tissue types. We believe that quantitative MRI, exploiting T_2 and ADC, will have potential clinical impact in the management of acute stroke patients, allowing an objective tissue-state evaluation of ischaemic parenchyma. The use of both quantitative T_2 and DWI/FLAIR mismatch would represent a shift towards the use of tissue-based MRI indices to assess tissue state in stroke patients.

Acknowledgements

The study is funded by the Dunhill Medical Trust (grants R385/1114 and OSRP1/1006). Support by the National Institute for Health Research Oxford Biomedical Centre Programme, the National Institute for Health Research Clinical Research Network, and the Wellcome Trust Institutional Strategic Support Fund (2015-2015) are acknowledged. We acknowledge the support of the National Institute for Health Research Clinical Research Network (NIHR CRN). We wish to acknowledge the facilities provided by Oxford Acute Vascular Imaging Centre.

REFERENCES

Bamford J, Sandercock P, Dennis M, Burn J and Warlow C 1991 Classification and natural history of clinically identifiable subtypes of cerebral infarction *Lancet* **337** 1521-6

Bristow M S, Simon J E, Brown R A, Eliasziw M, Hill M D, Coutts S B, Frayne R, Demchuk A M and Mitchell J R 2005 MR perfusion and diffusion in acute ischemic stroke: human gray and white matter have different thresholds for infarction *J Cereb Blood Flow Metab* **25** 1280-7

Burgess R E and Kidwell C S 2011 Use of MRI in the assessment of patients with stroke *Curr Neurol Neurosci Rep* **11** 28-34

Busza A L, Allen K L, King M D, van Bruggen N, Williams S R and Gadian D G 1992 Diffusion-weighted imaging studies of cerebral ischemia in gerbils. Potential relevance to energy failure *Stroke* **23** 1602-12

Chen C, Bivard A, Lin L, Levi C R, Spratt N J and Parsons M W 2017 Thresholds for infarction vary between gray matter and white matter in acute ischemic stroke: A CT perfusion study *J Cereb Blood Flow Metab* **in press** 271678X17744453

Grohn O H, Kettunen M I, Penttonen M, Oja J M, van Zijl P C and Kauppinen R A 2000 Graded reduction of cerebral blood flow in rat as detected by the nuclear magnetic resonance relaxation time T2: a theoretical and experimental approach *J Cereb Blood Flow Metab* **20** 316-26

Hjort N, Butcher K, Davis S M, Kidwell C S, Koroshetz W J, Röther J, Schellinger P D, Warach S and Østergaard L 2005 Magnetic resonance imaging criteria for thrombolysis in acute cerebral infarct *Stroke* **36** 388-97

Hossmann K A 1994 Viability thresholds and the penumbra of focal ischemia *Ann Neurol* **36** 557-65

Jenkinson M and Smith S 2001 A global optimisation method for robust affine registration of brain images *Med Image Anal* **5** 143-56

Jokivarsi K T, Hiltunen Y, Grohn H, Tuunanen P, Grohn O H and Kauppinen R A 2010 Estimation of the onset time of cerebral ischemia using T1ρ and T2 MRI in rats *Stroke* **41** 2335-40

Kauppinen R A 2014 Multiparametric magnetic resonance imaging of acute experimental brain ischaemia *Prog NMR Spectr* **80** 12-25

Kettunen M I, Grohn O H, Silvennoinen M J, Penttonen M and Kauppinen R A 2002 Quantitative assessment of the balance between oxygen delivery and consumption in the rat brain after transient ischemia with T2 -BOLD magnetic resonance imaging *J Cereb Blood Flow Metab* **22** 262-70

Knight M J, McGarry B L, Rogers H J, Jokivarsi K T, Grohn O H and Kauppinen R A 2015 A spatiotemporal theory for MRI T2 relaxation time and apparent diffusion coefficient in the brain during acute ischaemia: Application and validation in a rat acute stroke model *J Cereb Blood Flow Metab* **36** 1232-43

Kranz P G and Eastwood J D 2009 Does diffusion-weighted imaging represent the ischemic core? An evidence-based systematic review *AJNR Am J Neuroradiol* **30** 1206-12

Kumura E, Graf R, Dohmen C, Rosner G and Heiss W D 1999 Breakdown of calcium homeostasis in relation to tissue depolarization: comparison between gray and white matter ischemia *J Cereb Blood Flow Metab* **19** 788-93

Li F, Han S S, Tatlisumak T, Liu K F, Garcia J H, Sotak C H and Fisher M 1999 Reversal of acute apparent diffusion coefficient abnormalities and delayed neuronal death following transient focal cerebral ischemia in rats *Ann Neurol* **46** 333-42

McGarry B L, Rogers H J, Knight M J, Jokivarsi K T, Sierra A, Grohn O H and Kauppinen R A 2016 Stroke onset time estimation from multispectral quantitative magnetic resonance imaging in a rat model of focal permanent cerebral ischemia *Int J Stroke* **11** 677-82

McKean J W and Schrader R M 1984 A comparison of methods for studenttizing the samle median *Comm Stats, Simul Comput* **13** 751-73

Moseley M E, Cohen Y, Mintorovitch J, Chileuitt L, Shimizu H, Kucharczyk J, Wendland M F and Weinstein P R 1990 Early detection of regional cerebral ischemia in cats: comparison of diffusion- and T2-weighted MRI and spectroscopy *Magn Reson Med* **14** 330-46

Norton T J T, Pereyra M, Knight M J, McGarry B M, Jokivarsi K T, Grohn O H J and Kauppinen R A 2017 Stroke onset time determination using MRI relaxation times without non-ischaemic reference in a rat stroke model *Biomed Spectrosc Imaging* **6** 25-35

Pierpaoli C, Alger J R, Righini A, Mattiello J, Dickerson R, Des Pres D, Barnett A and Di Chiro G 1996 High temporal resolution diffusion MRI of global cerebral ischemia and reperfusion *J Cereb Blood Flow Metab* **16** 892-905

Price R M and Bonett D G 2001 Estimating the variance of sample median *J Stats Comput Simulat* **68** 295-305

Siemonsen S, Mouridsen K, Holst B, Ries T, Finsterbusch J, Thomalla G, Ostergaard L and Fiehler J 2009 Quantitative T2 values predict time from symptom onset in acute stroke patients *Stroke* **40** 1612-6

Sotak C H 2002 The role of diffusion tensor imaging in the evaluation of ischemic brain injury: A review *NMR Biomed* **15** 561-9

Thomalla G, Cheng B, Ebinger M, Hao Q, Tourdias T, Wu O, Kim J S, Breuer L, Singer O C, Warach S, Christensen S, Treszl A, Forkert N D, Galinovic I, Rosenkranz M, Engelhorn T, Köhrmann M, Endres M, Kang D W, Dousset V, Sorensen A G, Liebeskind D S,

Fiebach J B, Fiehler J and Gerloff C 2011 DWI-FLAIR mismatch for the identification of patients with acute ischaemic stroke within 4.5 h of symptom onset (PRE-FLAIR): a multicentre observational study *Lancet Neurol* **10** 978-86

Thomalla G, Rossbach P, Rosenkranz M, Siemonsen S, Krützelmann A, Fiehler J and Gerloff C 2009 Negative fluid-attenuated inversion recovery imaging identifies acute ischemic stroke at 3 hours or less *Ann Neurol* **65** 724-32

Thomalla G, Simonsen C Z, Boutitie F, Andersen G, Berthezene Y, Cheng B, Cheripelli B, Cho T H, Fazekas F, Fiehler J, Ford I, Galinovic I, Gellissen S, Golsari A, Gregori J, Gunther M, Guibernau J, Hausler K G, Hennerici M, Kemmling A, Marstrand J, Modrau B, Neeb L, Perez de la Ossa N, Puig J, Ringleb P, Roy P, Scheel E, Schonewille W, Serena J, Sunaert S, Villringer K, Wouters A, Thijs V, Ebinger M, Endres M, Fiebach J B, Lemmens R, Muir K W, Nighoghossian N, Pedraza S, Gerloff C and Investigators W-U 2018 MRI-guided thrombolysis for stroke with unknown time of onset *N Engl J Med* **379** 611-22

Welch K M, Windham J, Knight R A, Nagesh V, Hugg J W, Jacobs M, Peck D, Booker P, Dereski M O and Levine S R 1995 A model to predict the histopathology of human stroke using diffusion and T2-weighted magnetic resonance imaging *Stroke* **26** 1983-9

Zhang Y, Brady M and Smith S 2001 Segmentation of brain MR images through a hidden Markov random field model and the expectation-maximization algorithm *IEEE Trans Med Imaging* **20** 45-57

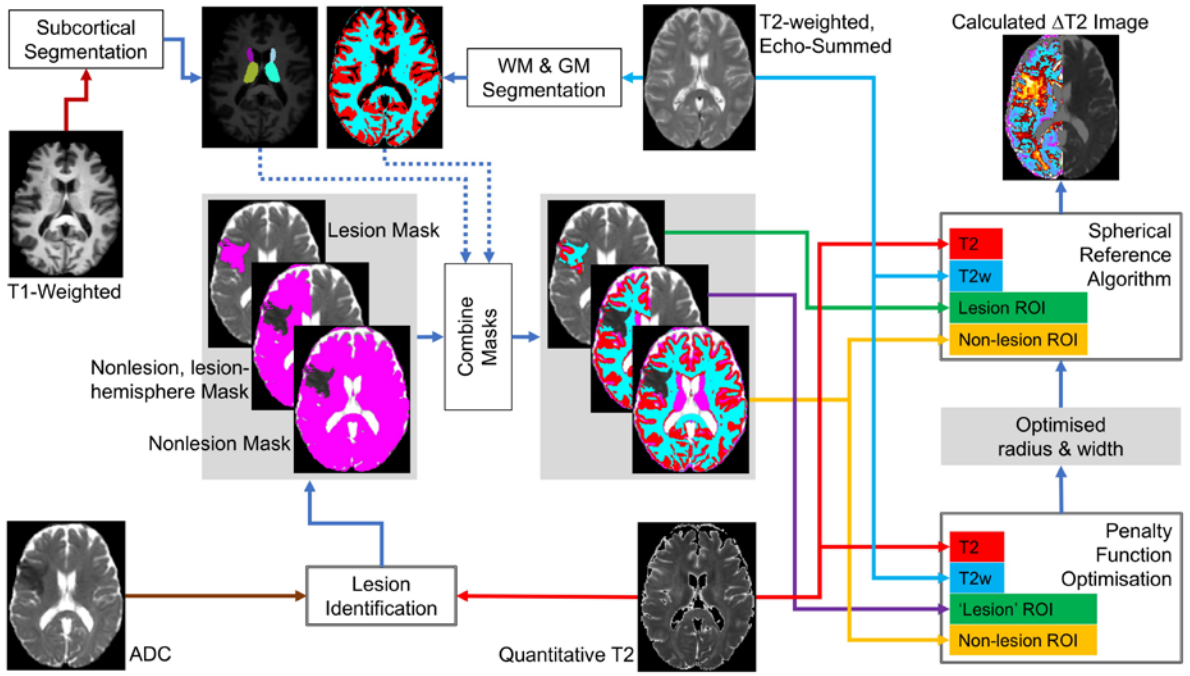

Figure 1. Flowchart showing the overall process of obtaining med(ΔT_2) for the lesion, and a calculated ΔT_2 image via the spherical reference method.

The illustrated process begins with the four MNI-registered, brain-extracted, input images: ADC, T_2-weighted (echo-summed), quantitative T_2, and T_1-weighted. Stage 1) Lesion Identification. ADC and T_2 images are used to identify the ischaemic lesion and create three masks: the lesion mask; the non-lesion mask (normal tissue without CSF); the non-lesion, lesion-hemisphere mask (normal tissue in the hemisphere of the lesion). Stage 2) Segmentation. GM and WM segmentations are produced from the T_2-weighted image, and a subcortical structure segmentation is produced from the T_1-weighted image. Stage 3) Mask Combination. If GM and WM tissue is to be studied separately, the subcortical segmentation masks are logically removed from the GM and WM segmentation masks, and the resulting masks are logically combined with the three masks of stage (1) to produced cortical GM and WM versions (see centre grey square of the flowchart). Stage 4) Penalty Function Optimisation. The spherical reference algorithm (inputs are T_2 and T_2-weighted images) is executed many times in order optimise the penalty function radius and width. This is achieved by minimising $\mathrm{MAD}(\Delta T_2) + 5|\mathrm{med}(\Delta T_2)|$, where ΔT_2 is calculated between the voxels of the non-lesion, lesion-hemisphere mask and the contralateral hemisphere voxels of the non-lesion mask. Stage 5) Spherical Reference Algorithm. Using the optimised penalty function radius and width from stage (4), and via the T_2 and T_2-weighted images, med(ΔT_2) is calculated for the lesion, using the lesion and non-lesion masks (or their segmented versions). A ΔT_2 image (shown in the top-right of the figure) can be produced by replacing the lesion mask with a lesion-hemisphere mask (not shown in the figure).

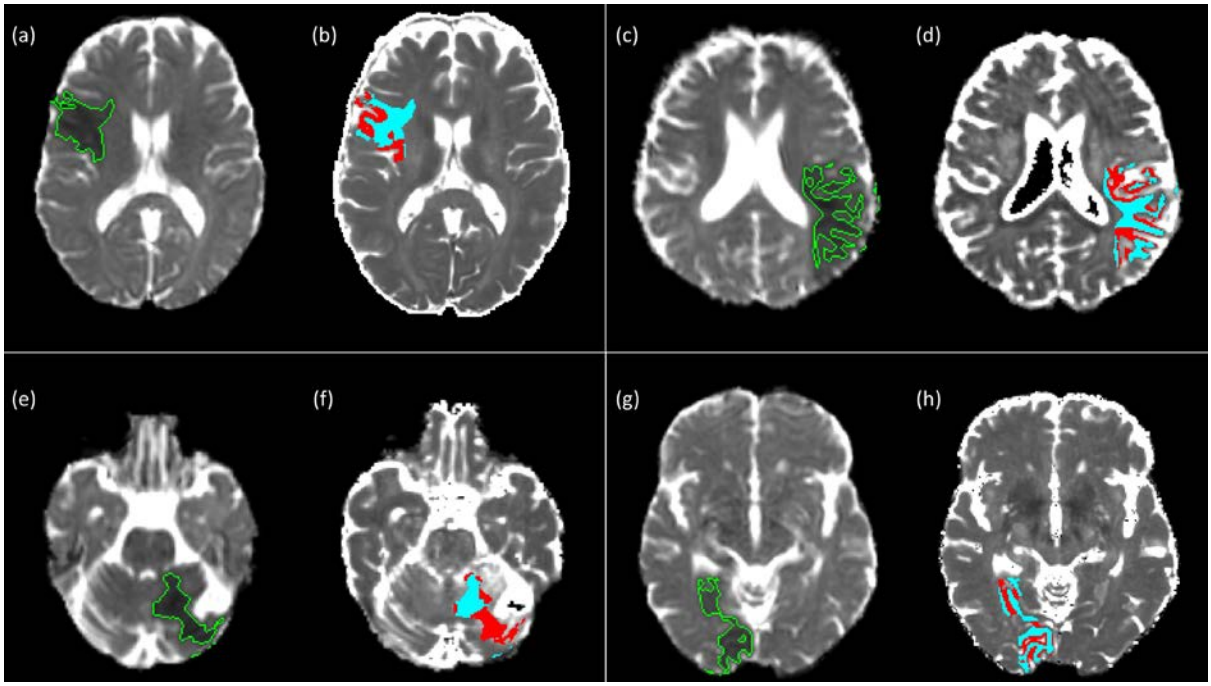

Figure 2. Examples of ADC images (a, c, e, g) with lesions demarcated, and quantitative T_2 images (b, d, f, h) with lesions segmented into WM (blue) and GM (red).

Panels (a, b): NIHSS at admission, 18; patient age, 45; stroke classification, TACS; onset time, 415 min. Panels (c, d): NIHSS at admission, 10; patient age, 57; stroke classification, LACS; onset time, 569 min. Panels (e, f): NIHSS at admission, 3; patient age, 86; stroke classification, POCS; onset time, 408 min. Panels (g, h): NIHSS at admission, 5; patient age, 80; stroke classification, POCS; onset time, 338 min.

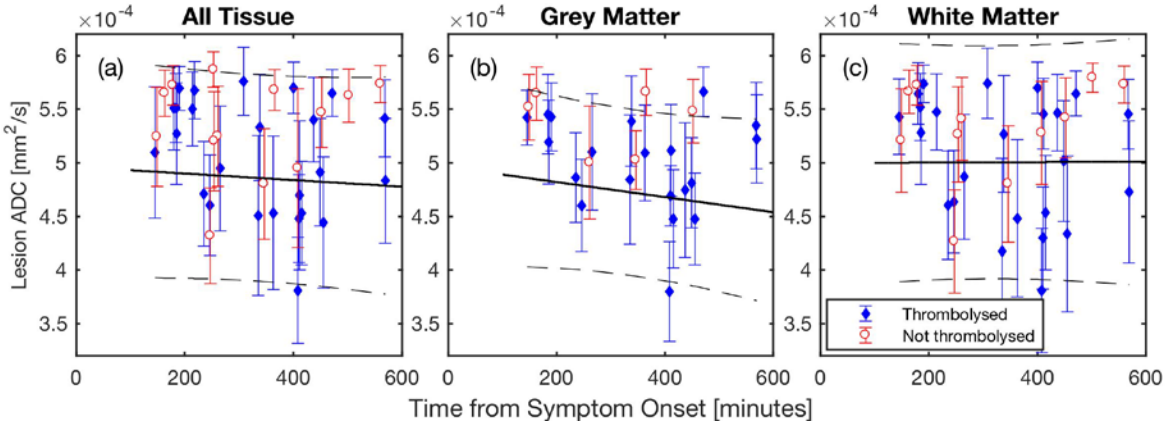

Figure 3. Lesion ADC values. The solid black line is the linear regression with observational 95% confidence intervals displayed by dashed black lines. The displayed error bars are the median absolute deviations. Regression results are given in Table 3.

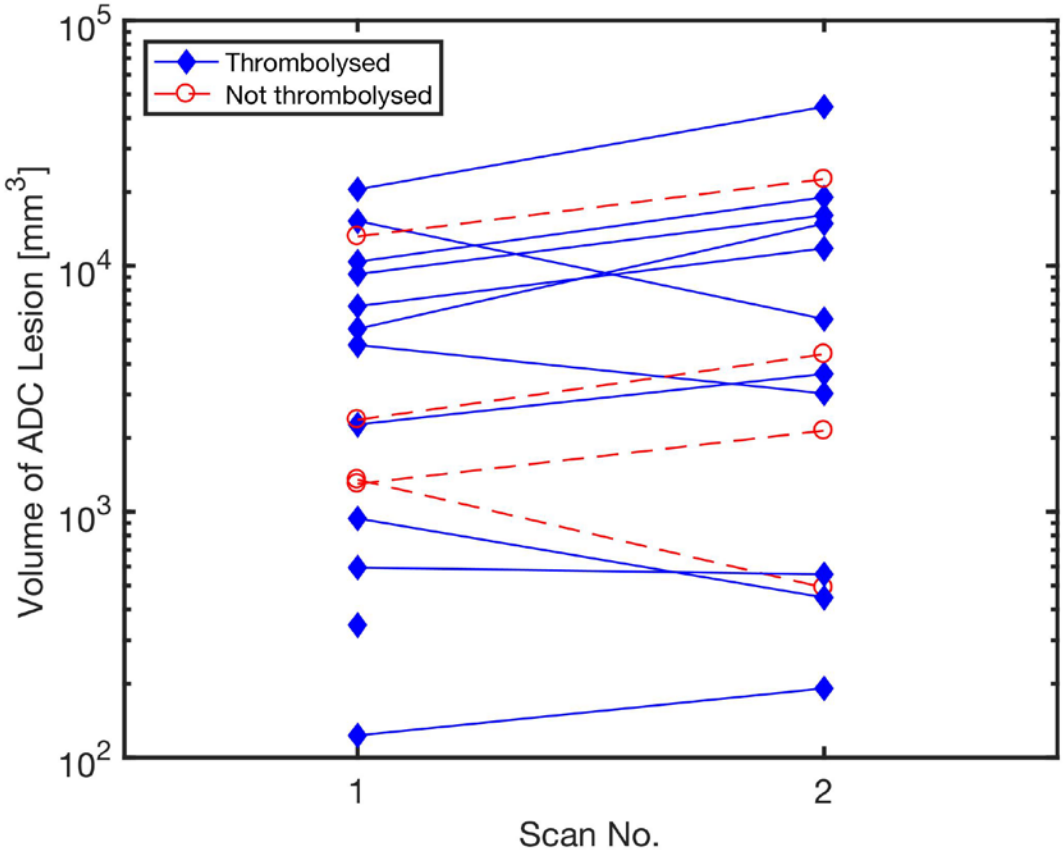

Figure 4. ADC lesion volumes (in mm^3) for the subset of patients with both a hyperacute scan (scan 1) and a follow-up scan (scan 2).

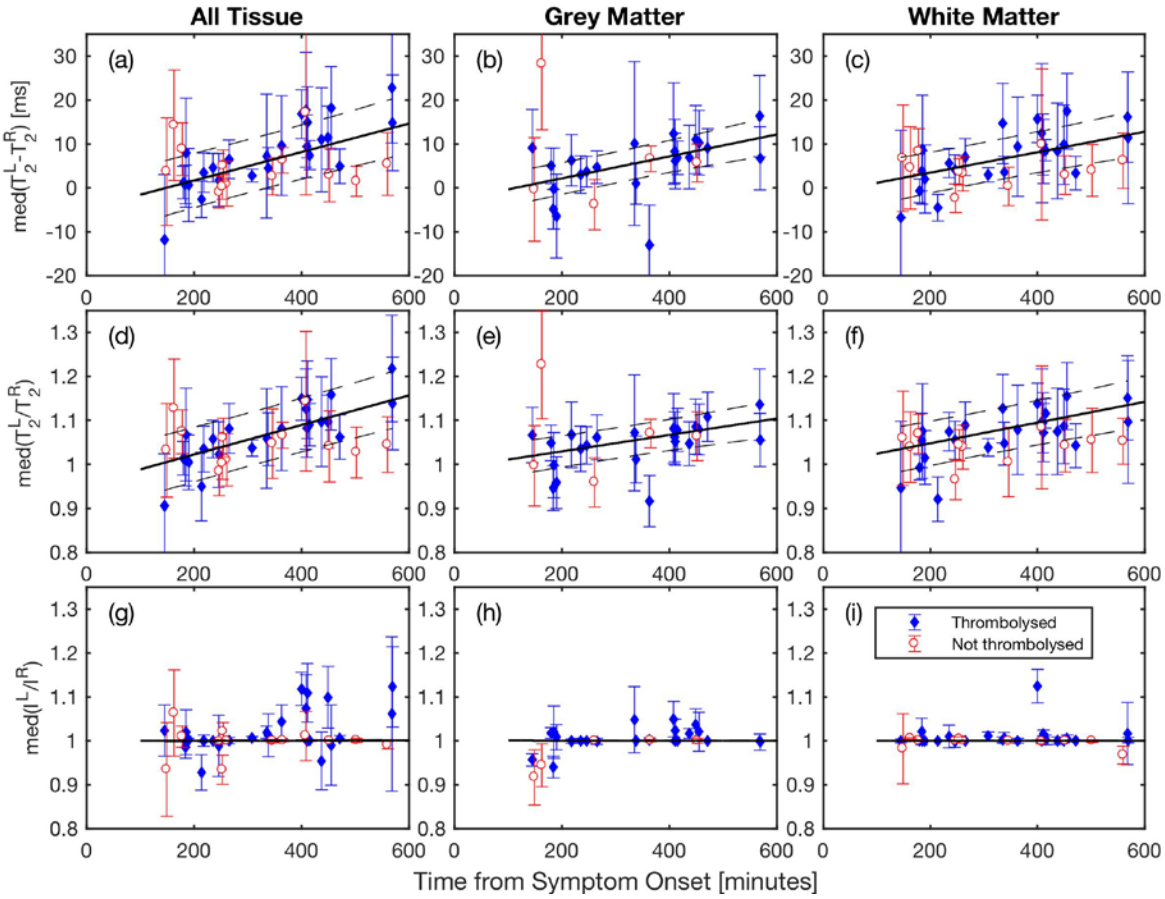

Figure 5. Spherical Reference method regressions for All Tissue, GM and WM lesions.

The solid black line is the linear regression with observational 95% confidence intervals displayed by dashed black lines. The 'error' bars displayed in the plots are the median absolute deviations (MADs) and represent the spread of values within the lesion or, alternatively, can be regarded as representing the tissue-state heterogeneity of the lesion. Regression results are given in Table 4.

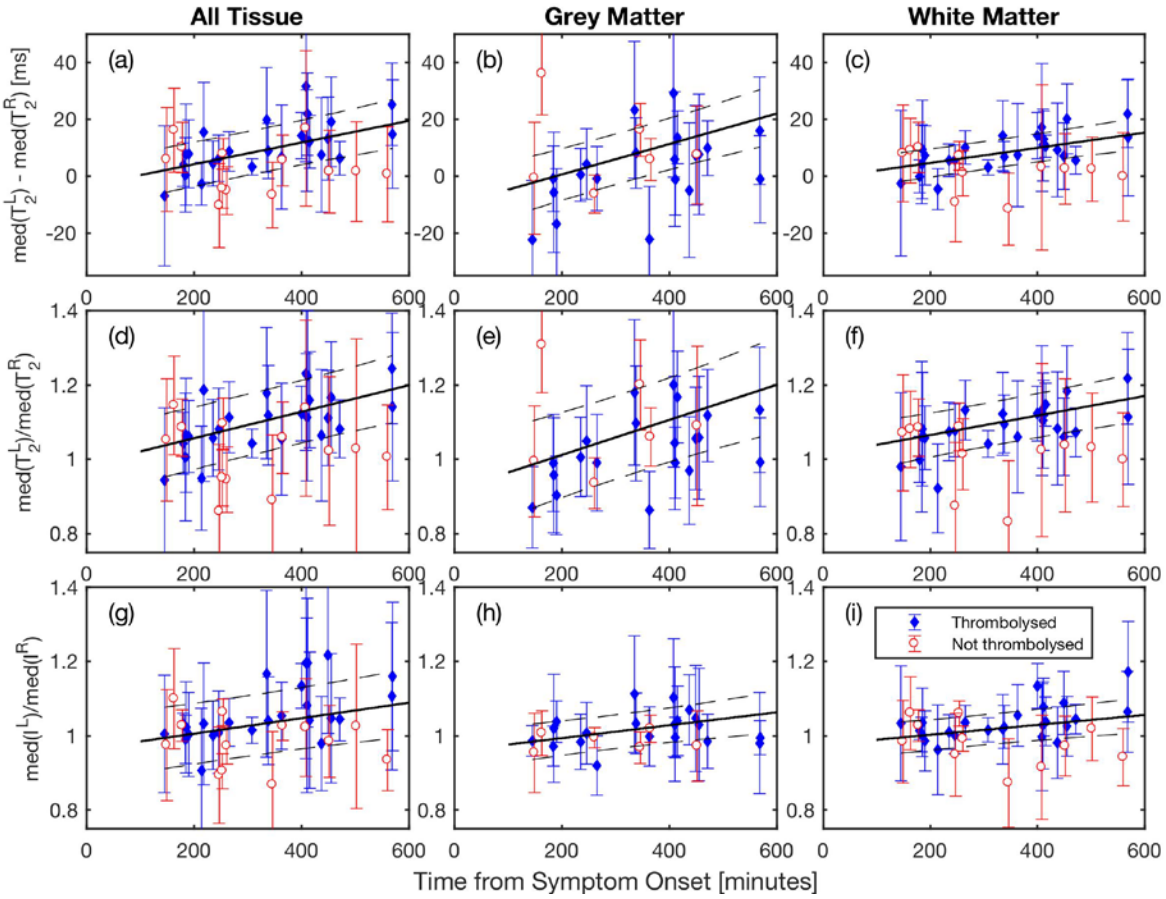

Figure 6. Mirror Reference method regressions for All Tissue, GM and WM lesions.

The solid black line is the linear regression with observational 95% confidence intervals displayed by dashed black lines. The 'error' bars depicted in the plots are the propagated MADs (see Methods section) from the lesion and contralateral regions. Regression results are given in Table 4.

Table 1. Patient data presented for the whole cohort in the hyperacute phase (all hyperacute patients) and for the subset who also received a follow-up MRI scan. Ranges presented in the table in parentheses are in the format: median (minimum – maximum).

Variable	All Hyperacute Data	Subset with Both Hyperacute and Follow-up Scans
Patients, n (% overall cohort)	38 (100%)	16 (42.1%)
Female, n (% group)	12 (31.6%)	5 (31.3%)
Scan site, n (% group)		
Bristol	19 (50.0%)	3 (18.8%)
Glasgow	15 (39.5%)	11 (68.8%)
Oxford	4 (10.5%)	2 (12.5%)
Age	68 (31 – 87)	68 (45 – 87)
Received r-tPA before MRI, n(% group)	25 (65.8%)	12 (75.0%)
Median time from rtPA to MRI (h:min)	3:17 (0:29 – 7:18)	4:12 (0:38 – 7:18)
Median time from onset to MRI (h:min)	5:38 (2:25 – 9:29)	6:52 (3:04 – 9:29)
Days from onset to follow-up MRI	-	1 (1 – 4)
NIHSS† on admission	6 (1 – 28)	8.5 (1 – 21)
Stroke subtype‡, n (% group)		
Lacunar (LACS)	15 (39.5%)	6 (37.5%)
Partial Anterior Circulation (PACS)	11 (28.9%)	5 (31.3%)
Posterior Circulation (POCS)	4 (10.5%)	1 (6.3%)
Total Anterior Circulation (TACS)	8 (21.1%)	4 (25.0%)
Left hemisphere stroke	15 (39.5%)	6 (37.5%)
ADC lesion volume [cm^3]		
Hyperacute	1.95 (0.04 – 97.51)	3.57 (0.12 – 20.50)
Follow-up	-	4.01 (0 – 44.53)

†Scores on the National Institutes of Health Stroke Scale (NIHSS) range 0 – 42, with higher scores indicating greater severity. ‡Strokes classified according to the Oxford Stroke Classification Scale (Bamford *et al.*, 1991)

Table 2. MRI sequence details and acquisition parameters.

Site	T_2 Sequence	T_R [ms]	T_E [ms]	Resolution [mm^3]
Bristol	GRASE	3000	20, 40, 60, 80, 100	0.6×0.6×2.3
Glasgow	TSE	12500	9.5, 66, 123	1.7×1.7×2.0
Oxford	FSE	12000	7.7, 77, 177	1.8×1.7×2.0

Site	T_1 Sequence	T_R [ms]	T_E [ms]	Resolution [mm^3]	T_I [ms]	Flip Angle
Bristol	3D FFE	6.84	3.18	1.0×1.0×1.1	N/A	8°
Glasgow	MP-RAGE	2200	2.28	0.9×0.9×0.9	900	9°
Oxford	MP-RAGE	1800	4.55	1.5×1.5×1.0	900	8°

Site	Diffusion Sequence	T_R [ms]	T_E [ms]	Resolution [mm^3]	b-value [s/mm^2] (Multiplicity)	Independent Gradient Directions
Bristol	SE-EPI	3009	60.5	1.2×1.2×4.4	0 (1), 1000 (3)	3
Glasgow	SE-EPI	8000	90	0.9×0.9×2.0	0 (3), 1000 (20)	20
Oxford	SE-EPI	5300	91	1.8×1.8×5.0	0 (1), 1000 (1)	3

Table 3. Weighted linear regression results for the ADC within the lesion [see Figure 3(a) – (c)]. r^2 is the square of the correlation coefficient, RMSE is the root-mean-square error of the residuals, *p* is the two-tailed p-value, *n* is the number of data points. Errors in the intercept and gradient are the 95% confidence intervals.

Tissue	Intercept [mm^2/s]	Gradient [$mm^2/s/h$]	r^2	RMSE	*p*	*n*
All	$4.96\times10^{-4} \pm 0.44\times10^{-4}$	$-1.8\times10^{-6} \pm 7.7\times10^{-6}$	0.0065	4.69×10^{-5}	0.629	38
GM	$4.96\times10^{-4} \pm 0.54\times10^{-4}$	$-4.2\times10^{-6} \pm 9.1\times10^{-6}$	0.0369	3.68×10^{-5}	0.347	26
WM	$5.00\times10^{-4} \pm 0.46\times10^{-4}$	$0.1\times10^{-6} \pm 8.3\times10^{-6}$	2.1×10^{-5}	5.27×10^{-5}	0.979	35

Table 4. Weighted linear regression results for spherical reference [Figure 5(a) – (i)] and mirror reference [Figure 6(a) – (i)] approaches. The data are displayed in the same order as the Figure panels. *Units for median ΔT_2 (spherical reference) and the difference of median T_2 are ms. Ratios are dimensionless. Units for the gradients are quoted in the appropriate units per hour. r^2 is the square of the correlation coefficient, RMSE is the root-mean-square error of the residuals, p is the two-tailed p-value (testing the gradient against the null hypothesis), $p_{GM\text{-}WM}$ is the two-tailed p-value testing the hypothesis that the gradients for GM and WM are identical), n is the number of data points. Errors in the intercept and gradient are the 95% confidence intervals.

Method	Measure	Tissue	Intercept*	Gradient*	r^2	RMSE	p	$p_{GM\text{-}WM}$	n
Spherical Reference	Median ΔT_2	All	-4.8 ± 3.3	1.94 ± 0.61	0.534	2.96	1.91×10^{-7}		38
		GM	-2.8 ± 2.6	1.50 ± 0.52	0.583	1.68	3.62×10^{-6}	0.810	27
		WM	-1.2 ± 2.8	1.40 ± 0.54	0.460	2.21	5.71×10^{-6}		35
	Median T_2 ratio	All	0.955 ± 0.032	0.0202 ± 0.0058	0.583	0.0296	2.43×10^{-8}		38
		GM	0.992 ± 0.024	0.0112 ± 0.0045	0.514	0.0165	2.60×10^{-5}	0.438	27
		WM	1.001 ± 0.029	0.0142 ± 0.0056	0.445	0.0241	1.07×10^{-5}		35
	Median intensity ratio	All	0.9991 ± 0.0011	2.2×10^{-4} ± 2.2×10^{-4}	0.103	8.08×10^{-4}	0.049		38
		GM	1.0008 ± 0.0007	-9.2×10^{-5} ± 9.4×10^{-5}	0.139	3.16×10^{-4}	0.055	0.0689	27
		WM	0.9999 ± 0.0005	0.5×10^{-4} ± 1.2×10^{-4}	0.023	5.32×10^{-4}	0.383		35
Mirror Reference	Difference of median T_2	All	-3.4 ± 4.2	2.30 ± 0.83	0.465	3.73	2.42×10^{-6}		38
		GM	-10.1 ± 6.1	3.2 ± 1.1	0.592	4.21	4.30×10^{-6}	0.0311	26
		WM	-0.6 ± 2.9	1.60 ± 0.57	0.498	2.36	2.18×10^{-6}		35
	Ratio of median T_2	All	0.986 ± 0.041	0.0214 ± 0.0079	0.453	0.0403	3.65×10^{-6}		38
		GM	0.917 ± 0.073	0.028 ± 0.013	0.449	0.0531	1.80×10^{-4}	0.102	26
		WM	1.013 ± 0.033	0.0158 ± 0.0062	0.447	0.0284	1.13×10^{-5}		35
	Ratio of median intensities	All	0.964 ± 0.037	0.0125 ± 0.0076	0.238	0.0395	1.89×10^{-3}		38
		GM	0.959 ± 0.031	0.0104 ± 0.0061	0.344	0.0216	1.65×10^{-3}	0.612	26
		WM	0.976 ± 0.022	0.0080 ± 0.0046	0.279	0.0196	1.12×10^{-3}		35